

Radiogenic Neutron Yield Calculations for Low-Background Experiments

S. Westerdale^{a,1,*}, P. D. Meyers^a

^a*Department of Physics, Princeton University, Princeton, New Jersey 08544, USA*

Abstract

Nuclear recoil backgrounds are one of the most dangerous backgrounds for many dark matter experiments. A primary source of nuclear recoils is radiogenic neutrons produced in the detector material itself. These neutrons result from fission and (α, n) reactions originating from uranium and thorium contamination. In this paper, we discuss neutron yields from these sources. We compile a list of (α, n) yields for many materials common in low-background detectors, calculated using NeuCBOT, a new tool introduced in this paper, available at <https://github.com/shawest/neucbot>. These calculations are compared to computations made using data compilations and SOURCES-4A.

Keywords: dark matter, neutron backgrounds, (α, n) yields, NeuCBOT

1. Introduction

Dark matter detectors and other low-background experiments rely on various techniques to discriminate between electron and nuclear recoils. Liquid argon detectors such as DarkSide-50 [1] and DEAP-3600 [2] rely on pulse shape discrimination to differentiate between these recoil types with very high efficiency. Liquid xenon time projection chambers, such as XENON1T [3] and LZ [4], can also differentiate between electron and nuclear recoils by comparing the amount of ionization detected to the amount of scintillation light collected, while bolometers such as SuperCDMS [5] can compare ionization and phonon production to achieve this goal. Since Weakly Interacting Massive Particle (WIMP) dark matter models typically predict that dark matter will interact most strongly with nuclei, eliminating electron recoil backgrounds, which result from β^\pm and γ -ray interactions, can be very effective. However, nuclear recoil backgrounds remain problematic for such experiments.

Nuclear recoil backgrounds result from α -decays on the inner surface of the detector ejecting a nucleus into the active volume of the detector or from

neutrons scattering in the active volume. Neutrons are produced through interactions of cosmogenic muons and the surrounding environment or by radiogenic processes in the detector materials.

Cosmogenic neutrons are typically mitigated by moving a detector deep underground, where the muon flux is greatly reduced. External muon vetoes, as described in [6], can be used to further reduce these backgrounds. A detailed discussion of these neutron backgrounds is provided in [7]. The focus of this document will be radiogenic neutrons.

Radiogenic neutrons result from nuclear interactions within a given material, typically due to contamination of radioactive isotopes in the ^{232}Th , ^{238}U , and ^{235}U decay chains. These neutrons may scatter once in the sensitive volume of a detector and then leave, producing a signal identical to that expected from a WIMP. While external veto systems, such as the design discussed in [8, 6], may be able to eliminate these backgrounds, a quantitative description of the radiogenic neutron backgrounds in a detector is necessary for any low-background experiment to understand and minimize its backgrounds.

2. Decay Chains and Secular Equilibrium

In this discussion, we will focus on three decay chains: ^{232}Th , ^{238}U , and ^{235}U . We will assume

*Corresponding author

Email address: shawest@physics.carleton.ca (S. Westerdale)

¹Current address: Department of Physics, Carleton University, Ottawa, Ontario K1S 5B6, Canada

secular equilibrium in these chains, with a few exceptions.

Secular equilibrium may be broken where a long-lived gaseous isotope can emanate from a material, where manufacturing or purification processes may selectively remove some isotopes, or where the material may have been exposed to elements partway down a decay chain, such as may be the case for radon. If these isotopes or their precursors have half-lives longer than the scale of the experiment, it may not be appropriate to assume secular equilibrium for the entire decay chain. In these cases, we will divide the chains into sub-chains in which we expect secular equilibrium to be preserved with respect to the top of the sub-chain.

In particular, ^{238}U has a half-life of 4.5×10^9 years and decays to ^{226}Ra , with a half-life of 1600 years, through four intermediate isotopes. Since ^{234m}Pa , one of the precursors of ^{226}Ra , emits a 1 MeV γ -ray that can be measured experimentally and ^{226}Ra has a 186 keV γ -ray, we split the ^{238}U decay chain into an upper and lower chain, defining all isotopes before ^{226}Ra to be in the upper chain, and ^{226}Ra and its progeny to be in the lower chain. Furthermore, since ^{210}Pb has a half-life of 22.2 years, far longer than its precursors, excess ^{210}Pb may accumulate in materials due to ^{222}Rn exposure in the air, causing secular equilibrium to be broken once again. Therefore, we account for the ^{210}Pb decay chain, consisting of ^{210}Pb and its progeny.

Throughout this document, we will discuss neutron yields in terms of neutrons produced per decay of the top of the decay chain. For a decay chain in secular equilibrium, this includes neutrons produced by all of the isotopes in this chain, weighted by the relevant branching ratios.

3. Direct Neutron Emission and Spontaneous Fission

While the primary focus of this document will be on neutrons produced by the (α, n) process, it is worth drawing attention to two other processes that produce radiogenic neutrons.

^{214}Bi α -decays to ^{210}Tl with a branching ratio of 0.021%, which then β -decays to ^{210}Pb . There is a 0.007% chance that this β -decay will go to an excited state of ^{210}Pb , which decays by emitting a 200–260 keV neutron to ^{209}Pb [9]. Due to these branching ratios, we expect to see these neutrons in $\sim 1.5 \times 10^{-8}$ of all decays of the lower ^{238}U chain.

Heavy nuclei that ordinarily α -decay may instead fission into smaller nuclei. When this happens, many particles may be ejected as well, including several MeV-scale γ -rays and some number of neutrons. The distribution of the number of γ -rays produced is discussed in [10], and the distribution of the number of neutrons emitted is discussed in [11]. These studies showed that the number of neutrons emitted in the spontaneous fission of ^{238}U can be modeled by a Gaussian distribution with a cutoff at 0, a mean of 2.05 ± 0.04 , and a standard deviation of 1.04 ± 0.03 .

These fission reactions are described in Table 1, which summarizes the spontaneous fission branching ratio BR_{SF} , the mean neutron kinetic energy $\langle E \rangle$, the mean neutron multiplicity $\langle \nu \rangle$, and the total number of neutrons produced per second per Becquerel of each decay chain for each isotope in these chains that may undergo spontaneous fission.

Table 1: Spontaneous fission branching ratios, mean neutron energies in MeV, mean neutron multiplicities, and neutron yields in n/s/Bq, simulated using SOURCES-4A.

Chain	Iso.	BR_{SF}	$\langle E \rangle$	$\langle \nu \rangle$	Yield
^{232}Th	^{232}Th	1.4E-11	1.7	2.1	3.0E-11
^{238}U	^{238}U	5.4E-07	1.8	2.0	1.1E-06
	^{234}U	1.2E-11	2.0	1.8	2.2E-11
	^{230}Th	5.3E-13	1.8	2.1	1.1E-12
^{235}U	^{235}U	2.0E-09	2.0	1.9	3.8E-09
	^{231}Pa	3.0E-12	2.0	1.9	5.8E-12

4. (α, n) Neutrons

The (α, n) reaction occurs predominantly in low-to-mid- Z materials with contamination from α -emitting isotopes. When these isotopes decay, the emitted α particle may capture on another nucleus in the material to form a compound nucleus, which may decay by neutron emission. The underlying physics of this reaction is discussed in more detail in [12].

While these neutrons are sometimes accompanied by a γ -ray, either correlated with the decay of the α -emitter or from the relaxation of the final nucleus, neutrons are also often produced alone. This possibility may make (α, n) neutrons particularly troublesome backgrounds, as there may be no accompanying signal to help tag the neutron. The rest of this document will therefore be focused on calculating (α, n) yields, including the introduction

of NeuCBOT as a tool for calculating these yields (see Section 4.2). In order to benchmark NeuCBOT against other standards, we will calculate (α, n) yields for several materials using NeuCBOT and compare these yields to calculations performed using measured yields on individual isotopes (see Section 4.3) as well as yields and neutron energy spectra predicted by SOURCES-4A (see Section 4.4).

4.1. Materials Considered

Table 2: Material compositions used in (α, n) calculations.

Material	Composition (% mass)				
Acrylic	H	C	O		
	8.1	60.0	31.9		
Alumina	Al	O			
	52.9	47.1			
Aluminum	Al				
	100				
Argon	Ar				
	100				
Be-Cu Alloy	Be	Ni	Cu		
	0.4	1.8	97.8		
Borosilicate Glass					
Brass	Cu	Zn			
	63	37			
Cirlex	H	C	N	O	
	2.6	69.1	7.3	20.9	
Copper	Cu				
	100				
Fused Silica	Si	O			
	46.7	53.3			
Kovar	Fe	Ni	Co	Mn	Si
	52.5	29	17	0.3	0.2
	C	Al	Mg	Zr	Ti
	0.02	0.1	0.1	0.1	0.1
	Cu	Cr	Mo		
	0.2	0.2	0.2		
NUV-HD Silicon Photomultipliers	Si	O	Al	Ti	
	99.27	0.5	0.2	0.03	
Polyethylene	H	C	O		
	4.2	62.5	33.3		
PTFE	C	F			
	24.0	76.0			
Solder	Sn	Ag	Cu		
	96.5	3.0	0.5		
Stainless Steel	C	Cr	Mn	Ni	P
	0.04	18	2	8	0.05
	S	Si	N	Fe	
	0.03	1	0.1	70.9	
Titanium	Ti				
	100				
Viton	H	C	F		
	0.9	28.1	71.0		
Xenon	Xe				
	100				

The (α, n) reaction depends on both the energy of the α particle being emitted and the various nuclei

with which the emitted α interacts. It is therefore important to define the chemical compositions of the materials for which we are calculating (α, n) yields.

We summarize the chemical compositions used for these calculations in Table 2. For each element, we assume natural isotopic abundances as reported in [13]. Some of the materials in this table require additional elaboration.

Alumina is a material commonly used in ceramics and makes up the bulk of many electronic components.

Be-Cu alloy is commonly used in connectors. While there are multiple such alloys, the composition used here is the one reported by Materion [14] for the PROtherm material. Materion reports a 50% uncertainty in the mass fraction of beryllium, which dominates the (α, n) yield, and a 22% uncertainty in the mass fraction of nickel. Based on the uncertainties in the chemical composition reported by Materion, we estimate a $\sim 47\%$ uncertainty in the total (α, n) yield due to uncertainties in the chemical composition.

The composition of borosilicate glass was provided by Hamamatsu Photonics through private communications, and we were asked not to disseminate this information. While we cannot provide the actual composition here, the composition we assumed is that used by Hamamatsu in the stems (backplates with leads) of their R11065 photomultiplier tubes. The (α, n) yield of borosilicate glass is dominated by boron, followed by lithium and aluminum. Based on the uncertainties in the chemical composition reported by Hamamatsu, we estimate a 5.7% uncertainty in the total (α, n) yield due to uncertainties in the chemical composition.

There are several different alloys of brass. For these calculations, we assumed a chemical composition typical of the “common brass” alloy. The (α, n) yield of common brass is dominated by copper. Based on typical tolerances reported in the composition of common brass, we estimate a 6.3% uncertainty in the total (α, n) yield due to uncertainties in the chemical composition.

Cirlex is an adhesiveless Kapton (polyimide) laminate used in low-background circuit boards, and Viton is a fluoropolymer rubber that is commonly used to make o-rings. The chemical compositions used for these calculations are from the NIST ESTAR database [15]. We assume that the uncertainty in the chemical composition of these materials is small.

Kovar is a metal alloy designed to have the same thermal expansion coefficient as borosilicate glass. For this reason, it is used as the outer shell of some Hamamatsu photomultiplier tubes. The composition used for these calculations is reported by the Carpenter Technology Corporation [16]. The (α, n) yield of Kovar is dominated by iron and cobalt. Based on the uncertainties in the chemical composition reported in [16], we estimate a 0.01% uncertainty in the total (α, n) yield due to uncertainties in the chemical composition.

Silicon photomultipliers are an alternative technology to photomultiplier tubes. The chemical composition used for these calculations was provided by Fondazione Bruno Kessler, for their NUV-SD devices.

While there are many different solder alloys, lead-free solders are typically used for low-background applications in order to reduce the amount of α -emitting contamination. The solder composition used for these calculations is based on the SAC305 ALPHA-Lo[®] alloy produced by Pure Technology, which is used in the Indium3.2 lead-free solder produced by the Indium Corporation. The primary contributor to the (α, n) yield is copper. Based on uncertainties in the chemical composition reported by Pure Technology, we estimate a 0.02% uncertainty in the total (α, n) yield due to uncertainties in the chemical composition.

For stainless steel, we used the nominal composition of 304L stainless steel reported by [17], assuming all elements whose compositions are given as upper bounds are at their limits. The (α, n) yield is dominated by the contributions from iron and chromium. Based on the ranges provided for the concentrations of each constituent element, we estimate 3% uncertainty in the (α, n) yield due to uncertainties in the chemical composition.

4.2. Calculation using NeuCBOT

To determine the (α, n) yield of materials exposed to a given list of α particle energies or α -emitting nuclei, we have written a program that compiles output from TALYS [18] with nuclear decay information from the ENSDF database [19] and stopping power calculations from SRIM [20].

We call this program NeuCBOT (Neutron Calculator Based On TALYS). It can be downloaded at <https://github.com/shawest/neucbot>.

SRIM is a program written by Ziegler et al. for simulating ion propagation in materials, based on the work in [20].

TALYS is a general nuclear reaction simulation program that uses nuclear structure data and theoretical models to calculate nuclear reaction cross sections and emission spectra for a projectile particle at a given energy impinging upon a specific target nucleus. Validation of this code is discussed in [18].

While TALYS relies more heavily on theoretical models than, e.g., SOURCES-4A, discussed below, does, it has the advantage that it is not limited by the availability of data and can be used to simulate the (α, n) reaction for α particles of any energy impinging upon any target nucleus. This flexibility allows TALYS to be used to predict (α, n) yields where SOURCES-4A and direct measurements lack data.

Since (α, n) yields may vary a lot between different isotopes of a given element, we consider each isotope in the material separately. If isotope i has a number density equal to η_i , the yield $Y_i(E_\alpha, E_n)$ of neutrons at energy E_n by an α particle with energy E_α that travels a distance dx is given by

$$Y_i(E_\alpha, E_n) = \eta_i \sigma_i(E_\alpha, E_n) dx, \quad (1)$$

where $\sigma_i(E_\alpha, E_n)$ is the cross section for this particular interaction. If the material has a total density ρ , we define the mass stopping power as $S(E) = -\frac{1}{\rho} \frac{dE}{dx}$. Performing a change in variables and integrating over E_α as the α particle slows down gives

$$\begin{aligned} Y_i^\alpha(E_n) &= \frac{\eta_i}{\rho} \int_0^{E_\alpha} \frac{\sigma_i(E'_\alpha, E_n)}{S(E'_\alpha)} dE'_\alpha \\ &= \frac{N_A C_i}{A_i} \int_0^{E_\alpha} \frac{\sigma_i(E'_\alpha, E_n)}{S(E'_\alpha)} dE'_\alpha, \end{aligned} \quad (2)$$

where $Y_i^\alpha(E_n)$ denotes the thick-target yield of neutrons of energy E_n from a given α particle (of *initial* energy E_α) in the decay chain, N_A is Avogadro's number, C_i is the mass fraction of isotope i in the material, and A_i is the mass number of the isotope. The total yield for a material can then be found by summing over the yield of each of the isotopes

$$Y^\alpha(E_n) = \sum_i Y_i^\alpha(E_n). \quad (3)$$

If we wish to determine the neutron yield of a decay chain consisting of several α particles, we define P_α to be the probability of an α particle appearing in a decay of the decay chain, based on the branching ratio for the parent isotope being produced and

the branching ratio for the parent isotope to decay to an α particle of this E_α . The total yield of neutrons of energy E_n is then given by

$$Y(E_n) = \sum_{\alpha} P_{\alpha} Y^{\alpha}(E_n). \quad (4)$$

The total number of neutrons produced at any energy is the integral of $Y(E_n)$ over the entire neutron energy spectrum.

The output of TALYS is the (α, n) total cross section for an α particle of specified energy reacting with the specific target nucleus, the individual cross sections for each excited state that the daughter nucleus may occupy after the reaction, cross sections for each γ -ray that may be produced in this reaction, and the energy spectrum of outgoing neutrons. The last quantity is determined by energy and momentum conservation for each daughter nucleus energy level and the corresponding cross section.

TALYS performs all of its calculations at the specified α energy; it does not simulate the α particle slowing down. The output of TALYS is thus the σ_i terms in Equation 2. It is therefore necessary to integrate over the track of the α particle as it slows down. This treatment differs from that presented in [21], which uses the output of TALYS directly as the integral, resulting in neutron spectra that over-predict the rate of neutrons at higher energies compared to NeuCBOT and SOURCES-4A. It also introduces uncertainties in the total neutron yield calculation, though we have not observed a consistent trend compared to NeuCBOT.

We have compiled a library of (α, n) reaction cross sections and neutron spectra generated by TALYS for most naturally occurring isotopes for α particle energies ranging from 0–10 MeV in 10 keV increments. This range is the energy range of α decays in the naturally occurring uranium and thorium decay chains and is therefore the most relevant to computing (α, n) neutron background rates.

In order to calculate (α, n) yields for an arbitrary material, NeuCBOT allows the user to specify a material composition. The user may do so either by giving each isotope and its mass fraction in the material, or by specifying the elemental composition of the material and the mass fraction of each element. In the latter case, the natural abundance of each isotope is looked up from a table published in [13], and these abundances are used to determine the isotopic composition of the material. The mass

fractions and mass numbers of each isotope are used as C_i and A_i , respectively, in Equation 2.

The user may also specify either a list of incident α particle energies and their relative intensities, or a list of α -emitting isotopes and their relative probabilities of appearing. The latter case is useful for simulating decay chains; the specified probabilities may be chosen as the isotopes' probabilities of appearing in the decay chain. In this case, a list of α particle energies and branching ratios is looked up for each isotope from the ENSDF database [19]. To speed up future computations, ENSDF data files are saved into a local library, so they only need to be retrieved once. These α particle energies and probabilities are used to define E_α in Equation 2, and P_α in Equation 4, respectively.

Total neutron yields can be calculated by integrating over the full neutron energy spectrum or by integrating over the total cross sections calculated by TALYS. These two methods typically agree to within 1–5%, deviating primarily due to uncertainties introduced in the Riemann integration and the finite resolution imposed by the binning of the neutron energy spectrum. The total yields output by NeuCBOT are therefore provided by the integral over the total cross sections.

NeuCBOT calculates the neutron yield and energy spectrum for each α particle as it slows down in a material and interacts with each isotope present, assuming a homogeneous composition, using Equation 2. The mass stopping powers $S(E_\alpha)$ are read from a library generated by SRIM as the α is integrated over its track as it slows down. This integral is approximated with a Riemann sum. The total yield of all neutrons of energy E_n is then found by summing over α s and isotopes, as described by Equations 3 and 4.

Other information about the (α, n) reaction, including excited nuclear states and associated coincident γ -rays are included in the TALYS-generated database in NeuCBOT.

This code, along with several example neutron energy spectra and a description of much of the underlying physics, are discussed in much detail in [12]. Neutron yield calculations for several common detector materials are shown in Table 4. In this table, the $^{238}\text{U}_{\text{lower}}$ chain includes contributions from ^{210}Pb and below; the ^{210}Pb column lists these contributions separately for cases where equilibrium is broken.

4.3. Calculations from Measured Yields

Various groups have published compilations of measured (α, n) yields. In the present discussion, we will draw from the compilations made by [22, 23, 24] for elements between lithium and iron, and the compilation made by [25] for heavier metals.

As discussed in these compilations, these measurements are difficult to perform. As a result, these measurements report uncertainties in the range of 10–20%, and different groups measuring the (α, n) yield of the same isotopes often report yields differing by up to 40%.

For these calculations, we used the isotopic abundances reported in [13]. Nuclear decay data, including α energies and probabilities, are determined using the Evaluated Nuclear Structure Data Files (ENSDF) [19].

When combining measured or calculated thick-target neutron yields over several isotopes to determine the yield of a composite material, it is important to note that the mass stopping power relevant in determining the (α, n) yield of a material is that material’s stopping power. However, measurements made on individual elements are determined by the stopping power of that element alone. In other words, the denominator of Equation 2 is $S_i(E)$ for each individual isotope being summed over, while it is $S(E) = \sum_i S_i(E)$ for the composite material.

To account for this difference, we follow the prescription described in [22], and rewrite Equation 2 as

$$\begin{aligned} Y_i^\alpha &= \frac{N_A C_i}{A_i} \int_0^{E_\alpha} \frac{S_i(E'_\alpha)}{S(E'_\alpha)} \frac{\sigma_i(E'_\alpha, E_n)}{S_i(E'_\alpha)} dE'_\alpha \\ &\approx \frac{N_A C_i}{A_i} \frac{S_i(E'_\alpha)}{S(E'_\alpha)} \int_0^{E_\alpha} \frac{\sigma_i(E'_\alpha, E_n)}{S_i(E'_\alpha)} dE'_\alpha \quad (5) \\ &= C_i \frac{S_i(E'_\alpha)}{S(E'_\alpha)} \tilde{Y}_i^\alpha, \end{aligned}$$

where \tilde{Y}_i^α is the measured neutron yield for isotope i . The approximation in the second line relies on the assumption that $S_i(E'_\alpha)/S(E'_\alpha)$ is approximately constant as the α slows down—that is to say that the stopping power of each isotope in the material has approximately the same functional form and they differ only by a constant factor.

For this calculation, we assume Bragg’s law for the additivity of stopping powers for the compounds discussed here, which we expect to be a safe

assumption [22]. Heaton et al. estimate that the assumption that $S_i(E'_\alpha)/S(E'_\alpha)$ is approximately constant introduces an uncertainty $\sim 5\%$ for E_α in the range of 3–10 MeV, where (α, n) neutrons are most likely to be produced. However, the uncertainty is likely higher for lighter nuclei such as carbon and beryllium.

We use SRIM to calculate the stopping power of each individual element in the material. Heaton et al. estimate a $\sim 5\%$ uncertainty in the final neutron yield calculations obtained this way due to uncertainties in SRIM.

Table 3: Isotopes missing from the SOURCES-4A and data compilation calculations presented here. Where only a chemical symbol is given, all isotopes of that element are missing. Li data was only available in SOURCES-4A at low energies, and was included in the ^{210}Pb and ^{238}U upper chains.

Be-Cu Alloy	Data	^{61}Ni , ^{64}Ni
	SOURCES-4A	Be, ^{61}Ni
Borosilicate	Data	Ba
Glass	SOURCES-4A	Li, Ba
Brass	Data	^{67}Zn
	SOURCES-4A	Zn
Cirlex	SOURCES-4A	^{15}N
Kovar	Data	Cr, ^{47}Ti , ^{61}Ni , ^{64}Ni
	SOURCES-4A	Zr, Mo, ^{52}Cr , ^{53}Cr , ^{54}Cr
Solder	Data	Sn
	SOURCES-4A	Ag, Sn
Stainless Steel	Data	Cr, P, S, ^{61}Ni , ^{64}Ni
	SOURCES-4A	S, ^{15}N , ^{52}Cr , ^{53}Cr , ^{54}Cr , ^{61}Ni
Titanium	Data	^{47}Ti
Xenon	Data	Xe
	SOURCES-4A	Xe

The results of these calculations for several materials common in low-background experiments are summarized in Table 4, where they are compared to NeuCBOT calculations. While these results are derived from measured yields, they are limited by the availability of data. Table 3 summarizes the isotopes for which we were lacking data for each material whose calculations are presented here. Missing isotopes were omitted from these calculations. These calculations are limited by experimental uncertainties and the uncertainties related to stopping powers discussed above. Additionally, these calcu-

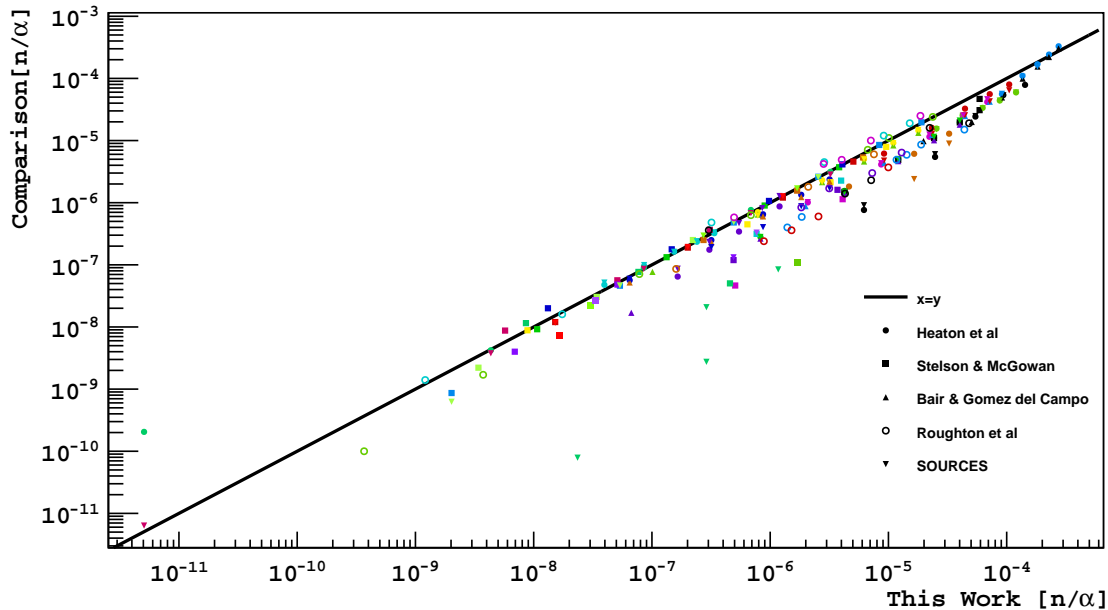


Figure 1: A scatter plot comparing the (α, n) yields calculated by NeuCBOT to various benchmark measurements and calculations. The straight black line is $x = y$, showing where this calculator agrees with a benchmark perfectly. Solid dots represent measurements presented in [22], squares in [25], triangles pointing up in [23], and hollow circles in [24]; triangles pointing down are calculations done by SOURCES-4A. Different colors correspond to measurements done on different target isotopes; progressions of points the same shape and color represent yields varying over energy.

lations do not provide neutron spectra, which may be necessary for simulating and understanding the neutron backgrounds.

4.4. Calculations using SOURCES-4A

In addition to comparing NeuCBOT neutron yields to the aforementioned data compilations, we used SOURCES-4A, developed by Los Alamos National Laboratory, to calculate (α, n) yields of various materials. Validation of SOURCES-4A and the underlying code is discussed at length in [26].

In summary, SOURCES-4A allows the user to specify a material composition and a set of α -emitting isotopes. It uses neutron yield measurements and stopping power calculations to simulate the (α, n) reaction in the target material. Since it is largely data-driven, it is subject to many of the same uncertainties discussed above. However, it also uses nuclear structure data to predict the neutron energy spectrum from these reactions.

The major limitation of calculations performed with SOURCES-4A is the availability of data. The default package distributed by Los Alamos National Laboratory does not contain (α, n) yield data for α

particle energies above 6.5 MeV, and many isotopes with significant neutron yields are missing entirely. For these calculation, we used the updates provided by [26, 27], which increase the energy range of available data and the set of isotopes for which there is data. While these extensions greatly increased the versatility of the SOURCES-4A code for performing these calculations, some isotopes were still missing entirely from the available dataset, and some isotopes were missing data at higher energies. The missing data is summarized in Table 3. Isotopes with missing data were omitted from the SOURCES-4A yield calculations in Table 4.

The results of these SOURCES-4A computations are summarized in Table 4. The often close agreement between yields predicted by SOURCES-4A and calculated from the published measurements should not be considered a strong independent verification of both methods; the data underlying both sets of yield calculations are the same for many isotopes, so agreement is not surprising. When SOURCES-4A and the data compilations disagree, SOURCES-4A often predicts lower yields than are observed.

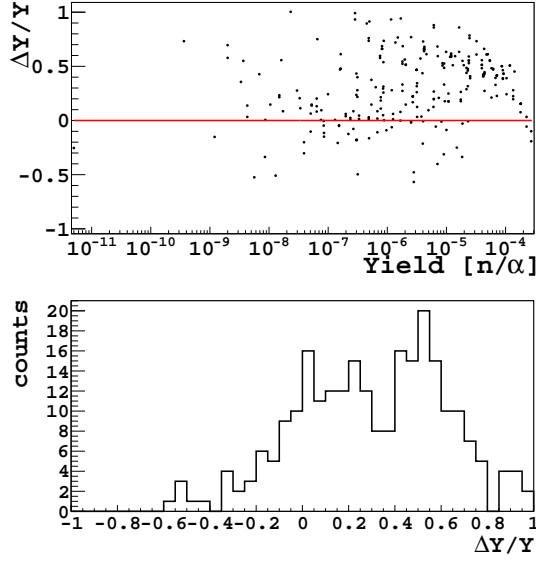


Figure 2: The distribution of the deviation of neutron yields calculated in this work compared to the various benchmark measurements and calculations for a range of isotopes with Z ranging from 3 to 49 and incident α energies ranging from 5 to 11 MeV. (Top) A scatter plot of the deviation versus the neutron yield. (Bottom) A histogram of all of the deviations, with a mean of 29.6% and an RMS of 31.9%.

4.5. NeuCBOT Validation and Comparisons

Figure 1 shows a scatter plot comparing various (α, n) yield measurements and SOURCES-4A calculations to NeuCBOT calculations. Qualitatively, this figure shows a strong correlation between data and NeuCBOT calculations over several orders of magnitude. We see that NeuCBOT tends to systematically predict higher yields. The biggest deviation is between the predictions for natural chromium made by SOURCES-4A and NeuCBOT, for which SOURCES-4A predicts yields 1–2 orders of magnitude lower than NeuCBOT. This deviation is likely due to the fact that (α, n) yields for ^{52}Cr , ^{53}Cr , and ^{54}Cr are missing from the SOURCES-4A dataset, all of which contribute significantly to the total (α, n) yield as predicted by TALYS. No (α, n) yield measurements were available for chromium in the dataset compilations used here.

In order to get a holistic view of how well NeuCBOT agrees with the other calculations and measurements, we define the fractional deviation of the yield to be $\Delta Y/Y = (Y_N - Y_i)/Y_N$, where Y_N is the yield computed by NeuCBOT and Y_i is the yield we are comparing it to.

A scatter plot showing the relationship between the fractional deviation and the yield and a dis-

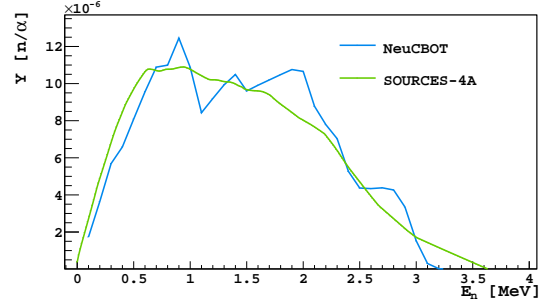


Figure 3: The (α, n) neutron energy spectrum for 6 MeV α particles impinging on a fluorine target, computed by NeuCBOT (blue) and by SOURCES-4A (green). For comparison, the SOURCES-4A spectrum has been scaled to have an equal integral to the NeuCBOT spectrum.

tribution of the fractional deviation are shown in Figure 2. In this distribution, we see that the fractional deviation has a mean value of 29.6% and an RMS of 31.9%.

We have found the the outgoing neutron energy spectra predicted by SOURCES-4A and NeuCBOT agree closely, with those generated by NeuCBOT predicting slightly more structure than is seen in the spectra predicted by SOURCES-4A. A comparison between the spectra predicted for fluorine can be seen in Figure 3, and more examples are provided in [12].

5. Conclusions

We introduce NeuCBOT, a new tool presented here that calculates (α, n) yields in arbitrary materials. We have used NeuCBOT to calculate (α, n) yields in many materials commonly used in low-background experiments due to ^{238}U , ^{235}U , and ^{232}Th contamination. We have compared these calculations to calculations made using measured yields and those performed by SOURCES-4A. While we found that NeuCBOT tends to predict yields systematically higher than these other two tools by $\sim 30\%$, it can provide (α, n) background rate estimates and spectra without being constrained by the availability of measurements.

For completeness, we also include a discussion of other radiogenic production rates due to these contaminants.

This code is available for general use. Documentation and the code can be downloaded at <https://github.com/shawest/neucbot>.

6. Acknowledgements

We would like to thank Pablo Mosteiro for help with the SOURCES-4A calculations. We would also like to thank Chris Stanford, Hao Qian, and Guangyong Koh for testing the code and providing valuable feedback.

References

- [1] P. Agnes, et al. (The DarkSide Collaboration), *Results from the first use of low radioactivity argon in a dark matter search*, [Phys. Rev. D](#), **93**, 081101 (2016).
- [2] M. G. Boulay (The DEAP Collaboration), *DEAP-3600 dark matter search at SNOLAB*, [J. Phys. Conf. Ser.](#), **375**, 012027 (2012), ISSN 1742-6596.
- [3] E. Aprile, et al. (The XENON1T Collaboration), *Physics reach of the XENON1T dark matter experiment*, [J. Cosmol. Astropart. Phys.](#), **2016**, 027 (2016).
- [4] D. C. Malling, et al., *After LUX: The LZ Program*, [arXiv:1110.0103](#) (2011).
- [5] R. Agnese, et al. (The SuperCDMS Collaboration), *Improved WIMP-search reach of the CDMS II germanium data*, [Phys. Rev. D](#), **92**, 072003 (2015).
- [6] P. Agnes, et al., *The veto system of the DarkSide-50 experiment*, [J. Instrum.](#), **11**, P03016 (2016), ISSN 1748-0221.
- [7] A. Empl, E. Hungerford, R. Jasim, and P. Mosteiro, *A Fluka study of underground cosmogenic neutron production*, [J. Cosmol. Astropart. Phys.](#), **2014**, 064 (2014), ISSN 1475-7516.
- [8] S. Westerdale, E. Shields, and F. Calaprice, *A prototype neutron veto for dark matter detectors*, [Astropart. Phys.](#), **79**, 10 (2016), ISSN 09276505.
- [9] M. Shamsuzzoha Basunia, *Nuclear Data Sheets for A = 210*, [Nuclear Data Sheets](#), **121**, 561 (2014), ISSN 0090-3752.
- [10] T. E. Valentine, *Evaluation of prompt fission gamma rays for use in simulating nuclear safeguard measurements*, [Ann. Nucl. Energy](#), **28**, 191 (2001), ISSN 03064549.
- [11] N. E. Holden and M. S. Zucker, *A reevaluation of the average prompt neutron emission multiplicity (nubar) values from fission of uranium and transuranium nuclides*, National Nuclear Data Center, Brookhaven National Laboratory (1984).
- [12] S. Westerdale, *A Study of Nuclear Recoil Backgrounds in Dark Matter Detectors*, Ph.D. thesis, Princeton University (2016).
- [13] P. De Bivre and P. D. P. Taylor, *Table of the isotopic compositions of the elements*, [Int. J. Mass Spectrom.](#), **123**, 149 (1993), ISSN 0168-1176.
- [14] Materion Brush Performance Alloys, [PROtherm™ Alloy Data Sheet](#).
- [15] M. J. Berger, J. Coursey, M. Zucker, and J. Chang, *Stopping-power and range tables for electrons, protons, and helium ions*, NIST Physics Laboratory (1998).
- [16] Carpenter Technology Corporation, [Kovar® Alloy](#).
- [17] Southwest Stainless & Alloy, [ALLOY INFORMATION AND SPECS](#).
- [18] A. Koning, S. Hilaire, and S. Goriely, *TALYS-1.6, Nuclear Reaction Program*, (2013).
- [19] J. K. Tuli, *Evaluated nuclear structure data file*, [Nucl. Instrum. Meth. A](#), **369**, 506 (1996), ISSN 0168-9002.
- [20] J. F. Ziegler and J. P. Biersack, *The stopping and range of ions in matter*, Springer (1985).
- [21] D. M. Mei, C. Zhang, and A. Hime, *Evaluation of induced neutrons as a background for dark matter experiments*, [Nucl. Instrum. Meth. A](#), **606**, 651 (2009), ISSN 0168-9002.
- [22] R. Heaton, H. Lee, P. Skensved, and B. C. Robertson, *Neutron production from thick-target (α , n) reactions*, [Nucl. Inst. Meth. A](#), **276**, 529 (1989).
- [23] J. K. Bair and J. Gomez del Campo, *Neutron Yields from Alpha-Particle Bombardment*, [Nucl. Sci. Eng.](#), **71**, 18 (1979), ISSN 00295639.
- [24] N. A. Roughton, et al., *Thick-target measurements and astrophysical thermonuclear reaction rates: α -induced reactions*, [At. Data Nucl. Data Tables](#), **28**, 341 (1983), ISSN 0092-640X.
- [25] P. H. Stelson and F. K. McGowan, *Cross Sections for (α ,n) Reactions for Medium-Weight Nuclei*, [Phys. Rev.](#), **133**, B911 (1964).
- [26] E. F. Shores, *Data updates for the SOURCES-4A computer code*, [Nucl. Instrum. Meth. B](#), **179**, 78 (2001), ISSN 0168-583X.
- [27] R. T. Perry and W. B. Wilson, *Neutron production from (α ,n) reactions and spontaneous fission in ThO_2 , UO_2 , and (U,Pu) O_2 fuels*, LA-8869-MS, (1981).

Table 4: (α, n) yields determined by NeuCBOT, compared data compilations and SOURCES-4A. Entries with a dash were not possible to calculate due to lacking data. The $^{238}\text{U}_{\text{lower}}$ chain *includes* equilibrium contributions from ^{210}Pb and below.

		^{232}Th	^{235}U	$^{238}\text{U}_{\text{upper}}$	$^{238}\text{U}_{\text{lower}}$	^{210}Pb
Acrylic	NeuCBOT	1.33×10^{-6}	1.42×10^{-6}	2.19×10^{-7}	9.72×10^{-7}	1.16×10^{-7}
	Data	9.11×10^{-7}	9.28×10^{-7}	1.07×10^{-7}	6.32×10^{-7}	6.46×10^{-8}
	SOURCES-4A	2.56×10^{-6}	2.81×10^{-6}	3.77×10^{-7}	1.10×10^{-6}	2.23×10^{-7}
Alumina	NeuCBOT	2.21×10^{-5}	2.01×10^{-5}	5.14×10^{-7}	1.38×10^{-5}	7.35×10^{-7}
	Data	8.54×10^{-6}	8.54×10^{-6}	2.11×10^{-7}	5.96×10^{-6}	2.82×10^{-7}
	SOURCES-4A	9.89×10^{-6}	8.59×10^{-6}	2.10×10^{-7}	2.00×10^{-6}	2.76×10^{-7}
Aluminum	NeuCBOT	4.53×10^{-5}	4.12×10^{-5}	1.00×10^{-6}	2.83×10^{-5}	1.49×10^{-6}
	Data	1.99×10^{-5}	1.19×10^{-5}	3.37×10^{-7}	1.19×10^{-5}	5.26×10^{-7}
	SOURCES-4A	1.96×10^{-5}	1.68×10^{-5}	3.21×10^{-7}	3.78×10^{-6}	4.99×10^{-7}
Argon	NeuCBOT	2.64×10^{-5}	1.72×10^{-5}	8.82×10^{-8}	1.41×10^{-5}	2.26×10^{-7}
	Data	—	—	—	—	—
	SOURCES-4A	2.22×10^{-5}	1.48×10^{-5}	1.77×10^{-7}	2.65×10^{-6}	2.32×10^{-7}
Be-Cu Alloy	NeuCBOT	6.22×10^{-6}	6.72×10^{-6}	1.58×10^{-6}	4.66×10^{-6}	7.59×10^{-7}
	Data	5.01×10^{-6}	5.26×10^{-6}	8.29×10^{-7}	3.61×10^{-6}	4.86×10^{-7}
	SOURCES-4A	2.48×10^{-7}	1.47×10^{-8}	1.10×10^{-6}	2.84×10^{-9}	4.89×10^{-7}
Borosilicate Glass	NeuCBOT	2.43×10^{-5}	2.56×10^{-5}	3.93×10^{-6}	1.76×10^{-5}	2.25×10^{-6}
	Data	1.33×10^{-5}	1.41×10^{-5}	2.25×10^{-6}	9.79×10^{-6}	1.32×10^{-6}
	SOURCES-4A	1.28×10^{-5}	1.40×10^{-5}	2.16×10^{-6}	5.99×10^{-6}	1.30×10^{-6}
Brass	NeuCBOT	3.06×10^{-7}	1.42×10^{-8}	6.52×10^{-14}	2.58×10^{-8}	5.72×10^{-13}
	Data	1.81×10^{-7}	1.19×10^{-8}	0	2.31×10^{-8}	0
	SOURCES-4A	1.59×10^{-7}	9.44×10^{-9}	0	1.82×10^{-9}	0
Cirlex	NeuCBOT	3.09×10^{-6}	2.57×10^{-6}	2.66×10^{-7}	2.01×10^{-6}	1.39×10^{-7}
	Data	1.64×10^{-6}	1.41×10^{-6}	1.20×10^{-7}	1.04×10^{-6}	7.26×10^{-8}
	SOURCES-4A	1.94×10^{-6}	1.77×10^{-6}	1.65×10^{-7}	5.32×10^{-7}	9.43×10^{-8}
Copper	NeuCBOT	3.86×10^{-7}	1.71×10^{-8}	0	3.17×10^{-8}	0
	Data	2.13×10^{-7}	1.47×10^{-8}	0	2.88×10^{-8}	0
	SOURCES-4A	2.53×10^{-7}	1.50×10^{-8}	0	2.90×10^{-9}	0
Fused Silica	NeuCBOT	1.81×10^{-6}	1.64×10^{-6}	7.58×10^{-8}	1.15×10^{-6}	7.91×10^{-8}
	Data	1.47×10^{-6}	1.37×10^{-6}	8.27×10^{-8}	9.41×10^{-7}	7.23×10^{-8}
	SOURCES-4A	1.73×10^{-6}	1.54×10^{-6}	1.06×10^{-7}	4.85×10^{-7}	8.55×10^{-8}
Kovar	NeuCBOT	1.22×10^{-6}	2.81×10^{-7}	3.22×10^{-9}	3.29×10^{-7}	4.05×10^{-9}
	Data	1.14×10^{-6}	2.62×10^{-7}	2.19×10^{-9}	3.31×10^{-7}	2.56×10^{-9}
	SOURCES-4A	1.16×10^{-6}	4.10×10^{-7}	2.28×10^{-8}	1.03×10^{-7}	1.38×10^{-8}
NUV-HD Silicon Photomultipliers	NeuCBOT	3.51×10^{-6}	3.07×10^{-6}	7.77×10^{-8}	2.16×10^{-6}	1.19×10^{-7}
	Data	2.63×10^{-6}	2.31×10^{-6}	6.45×10^{-8}	1.59×10^{-6}	9.24×10^{-8}
	SOURCES-4A	3.21×10^{-6}	2.67×10^{-6}	1.12×10^{-7}	7.46×10^{-7}	1.18×10^{-7}
Polyethylene	NeuCBOT	1.48×10^{-6}	1.58×10^{-6}	2.45×10^{-7}	1.08×10^{-6}	1.30×10^{-7}
	Data	1.01×10^{-6}	1.03×10^{-6}	1.19×10^{-7}	7.01×10^{-7}	7.18×10^{-8}
	SOURCES-4A	1.29×10^{-6}	1.35×10^{-6}	1.60×10^{-7}	4.82×10^{-7}	9.21×10^{-8}
PTFE	NeuCBOT	1.27×10^{-4}	1.31×10^{-4}	1.16×10^{-5}	8.85×10^{-5}	9.37×10^{-6}
	Data	9.26×10^{-5}	9.56×10^{-5}	8.15×10^{-6}	6.46×10^{-5}	6.33×10^{-6}
	SOURCES-4A	6.91×10^{-5}	7.35×10^{-5}	5.96×10^{-6}	2.54×10^{-5}	4.83×10^{-6}
Solder	NeuCBOT	2.53×10^{-9}	1.11×10^{-10}	0	2.06×10^{-10}	0
	Data	1.37×10^{-9}	9.53×10^{-11}	0	1.87×10^{-10}	0
	SOURCES-4A	1.64×10^{-9}	9.68×10^{-11}	0	1.87×10^{-11}	0
Stainless Steel	NeuCBOT	1.96×10^{-6}	4.42×10^{-7}	1.31×10^{-9}	5.52×10^{-7}	2.14×10^{-9}
	Data	1.25×10^{-6}	2.85×10^{-7}	1.04×10^{-9}	3.73×10^{-7}	1.43×10^{-9}
	SOURCES-4A	1.19×10^{-6}	2.78×10^{-7}	1.64×10^{-9}	4.60×10^{-8}	1.71×10^{-9}
Titanium	NeuCBOT	7.34×10^{-6}	2.58×10^{-6}	2.89×10^{-9}	2.81×10^{-6}	1.17×10^{-8}
	Data	6.30×10^{-6}	2.75×10^{-6}	0	2.60×10^{-6}	2.13×10^{-8}
	SOURCES-4A	6.08×10^{-6}	2.47×10^{-6}	5.86×10^{-9}	3.74×10^{-7}	1.56×10^{-8}
Viton	NeuCBOT	1.15×10^{-4}	1.19×10^{-4}	1.06×10^{-5}	8.07×10^{-5}	8.53×10^{-6}
	Data	8.44×10^{-5}	8.72×10^{-5}	7.43×10^{-6}	5.89×10^{-5}	5.77×10^{-6}
	SOURCES-4A	6.26×10^{-5}	6.66×10^{-5}	5.39×10^{-6}	2.30×10^{-5}	4.37×10^{-6}
Xenon	NeuCBOT	6.15×10^{-12}	1.24×10^{-14}	0	1.25×10^{-13}	0
	Data	—	—	—	—	—
	SOURCES-4A	—	—	—	—	—